nature biomedical engineering

Review article

https://doi.org/10.1038/s41551-026-01806-4

Engineering human multi-organ tissue chip niches for drug absorption, distribution, metabolism, excretion and toxicity prediction

Received: 20 December 2025

Accepted: 28 August 2026

Published online: 5 October 2026

Check for updates

Jiawei Li[1,2], Sofia Madrigal Gamboa[3,4], Jade T. Chao[5], Sarah C. Heilshorn[4] & Joseph C. Wu[1,2]

Predicting human drug responses in vitro remains a central challenge in drug development. Animal models have shown limited accuracy in recapitulating human drug absorption, distribution, metabolism, excretion and toxicity, which arise from coordinated activities across multiple organs. Multi-organ-on-a-chip systems (mOoCs) are a class of promising new approach methodologies that can reconstruct these inter-organ processes. Existing mOoCs have demonstrated proof of concept for inter-organ coupling but translation-ready systems remain out of reach. Two key challenges persist: how to preserve the distinct biochemical and biomechanical niches of each organ while enabling controlled exchange between them, and how to develop mOoCs into robust translation-ready systems. In this Review, we first summarize progress in niche-preserving engineering strategies developed within single-organ systems and outline how these components are integrated to reconstruct multi-organ niches. We then highlight scalable manufacturing and multimodal readouts as the basis for making mOoCs into robust, reproducible and data-rich technologies for drug response evaluation. In the future, the resulting human-relevant datasets are expected to interface with artificial intelligence workflows to accelerate next-generation drug discovery.

Drug discovery is a decade-long, multi-billion-dollar process that urgently awaits optimization to improve human health and economic efficiency. A central barrier is the limited predictive accuracy of human drug absorption, distribution, metabolism, excretion and toxicity (ADMET) properties from preclinical models. For instance, current preclinical animal models exhibit a median positive predictive value of 0.65 and negative predictive value of 0.5 across 108 oncology drug toxicity assessments[1]. This utility drops further because human biology diverges from other species in drug metabolic enzymes[2], neurodegenerative disease[3], immonology[4,5] and so on.

New approach methodologies (NAMs), encompassing advanced in vitro cultures, in silico algorithms and in chemico assays, have emerged to address these limitations by reconstituting human cell biology outside of animals and have attracted substantial attention from both academia[6–9] and regulatory agencies (the US Food and Drug Administration (FDA)[10], National Institutes of Health (NIH)[11] and Centers for Disease Control and Prevention (CDC)[12], and the K-Organoid Consortium[13]). With the rapid development of in vitro NAMs, such as human cell culture, organoids and organ-on-a-chip (OoC) systems, researchers have increased the in vitro modelling complexity of individual organs.

[1]Stanford Cardiovascular Institute, Stanford University School of Medicine, Stanford, CA, USA. [2]Division of Cardiovascular Medicine, Department of Medicine, Stanford University School of Medicine, Stanford, CA, USA. [3]Department of Mechanical Engineering, Stanford University, Stanford, CA, USA. [4]Department of Materials Science and Engineering, Stanford University, Stanford, CA, USA. [5]Greenstone Biosciences, Palo Alto, CA, USA.
e-mail: joewu@stanford.edu

https://doi.org/10.1038/s41551-026-01806-4

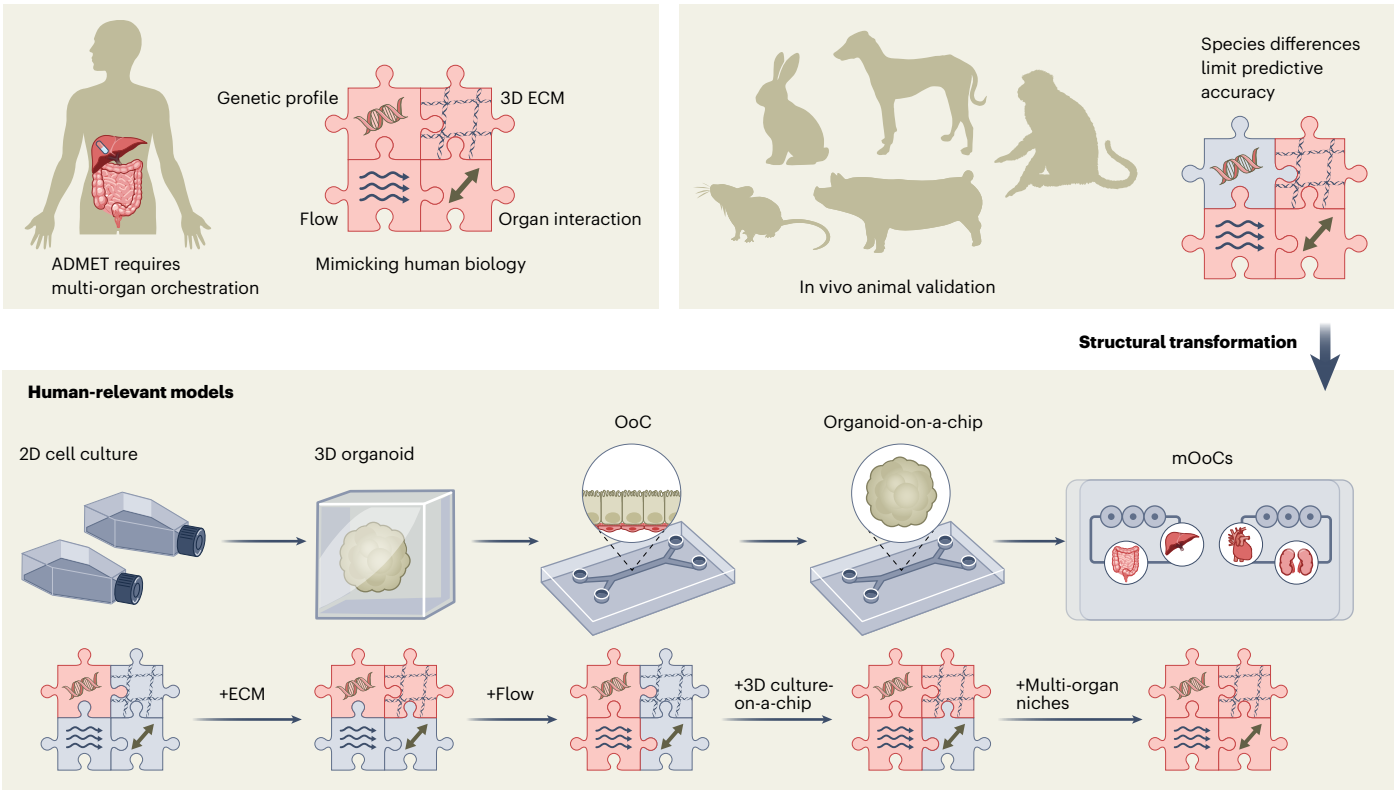


Fig. 1 | Structural transformation towards multi-organ NAM-based ADMET prediction. Human ADMET emerges from the orchestration of multiple organs rather than the simple sum of individual organ responses. Modelling human drug ADMET therefore requires a comprehensive recapitulation of the human genetic profile, 3D ECM, fluid flow and inter-organ interaction. Conventional preclinical animal models provide an in vivo physiological environment but interspecies genetic differences compromise the accuracy of predictions of human drug responses. Two-dimensional (2D) human cell culture has shown utility in specific applications. Over the past decade, 3D organoids and OoC systems have enhanced in vitro recapitulation by incorporating 3D matrices and fluidic flow, respectively. Organoids have also been integrated into OoCs. mOoC systems further recapitulate inter-organ interactions, providing an integrated model for investigating human drug ADMET in vitro.

Two-dimensional human cell models showed utility in specific applications, such as predicting drug permeability using the Caco-2 assay[14] and predicting cardiac arrhythmia using the hERG assay[15], but so far have failed to recapitulate the three-dimensional (3D) architecture of human tissues. Organoids partially addressed this problem by leveraging 3D cell self-organization and biochemical cocktails to establish miniature organs in vitro. Examples include stem cell-derived gastruloids that could capture early human cardiac and hepatic vascularization processes[16]. In addition, effusion-derived lung cancer organoids predicted matched clinical drug responses in advanced lung cancer with 83.3% overall accuracy[17]. Beyond cellular and structural complexity, OoC systems (also denoted as microphysiological systems) further address the spatial biomechanical cues of human physiology. By emulating the human fluidic environment in microfluidic chips, OoCs are cell culture devices that enable microlitre-volume laminar perfusion with controlled flow, shear stress and substance delivery[18]. Engineered mini-colon chips, for example, have modelled the spatio–temporal dynamics of human colorectal oncogenesis[19]. Together, these advances are considerably improving the spatio–temporal microenvironment modelling of individual organs (Fig. 1).

However, in vivo drug ADMET is not the simple sum of individual organ responses but rather emerges from inter-tissue and inter-organ metabolic coupling and signalling. Drug absorption, for example, is orchestrated by intestinal epithelium and gut microbiota. A systematic analysis of 271 oral drugs identified bacterial enzymes that could alter oral bioavailability and downstream tissue exposure[20]. Inter-organ metabolism is also related to drug toxicity. Terfenadine, a non-sedating antihistamine, is safe when metabolized normally by hepatic CYP3A4 but causes fatal arrhythmias when co-administered with CYP3A4 inhibitors that allow the parent compound to accumulate and block cardiac hERG channels[21]. These cases demonstrate that human-relevant ADMET prediction requires in vitro multi-organ systems that are capable of supporting continuous, systemic inter-organ exchange.

Multi-organ-on-a-chip systems (mOoCs) are beginning to address this need. Throughout this Review, OoC and mOoC denote single-organ- and multi-organ-on-a-chip systems, respectively, with organoid-on-a-chip and multi-organoid-on-a-chip regarded as their subsets. Compared to conditioned-medium approaches[22] and direct-contact assembloids[23], which capture inter-tissue interactions but lack individual niches and circulatory architectures, mOoCs enable continuous fluidic perfusion between distinct tissue compartments. For example, mOoC systems have been maintained for 4 weeks and enabled pharmacokinetic (PK) analysis of diclofenac metabolism[24]. Endothelium-connected mOoCs have been used to evaluate the PK of nicotine and cisplatin[25]. Gut–liver–brain mOoCs could identify disease-associated metabolic signatures in a Parkinson's disease model[26]. Despite the progress, the mOoCs available at present remain limited in their ability to preserve the distinct niche of each organ compartment while enabling controlled inter-organ exchange. Many existing systems homogenize media across compartments, lack vascular specialization and cannot efficiently maintain organ-specific microenvironments under continuous flow. Without niche-specific microenvironments, mature tissue phenotypes regress and organ-specific drug responses diverge from human physiology, undermining the ADMET predictions that mOoCs are intended to provide[27].

Another major challenge in developing organoids, OoCs and mOoCs is acquiring reliable and reproducible data. As 3D culture complexity increases, so does experimental variance. Existing mOoC

systems still lack standardized scalable manufacturing and the multimodal readouts required to generate reproducible human-relevant datasets at translational scale. Without robust data, even the most sophisticated mOoC cannot serve as a reliable translational platform for drug evaluation.

In this Review we focus on the two most critical engineering challenges required to make mOoCs translation-ready: how to preserve niche identity under controlled inter-organ exchange and how to make mOoCs into robust translation-ready platforms. We first summarize progress in niche-preserving engineering strategies developed within single-organ systems and outline how these components can be integrated to reconstruct multi-organ niches. We then highlight scalable manufacturing and multimodal readouts as the basis for transforming mOoCs into robust data-rich platforms for drug response evaluation.

Niche preservation under controlled inter-organ exchange

Biological systems maintain homeostasis and function through selective exchange, which is the controlled movement of molecules and cells between physiological compartments that preserves local identity while enabling coordinated communication[28]. To predict drug ADMET in vitro, mOoCs should construct distinct organ niches with selective exchange rather than rely on fluidic connectivity alone. We first review how the human body maintains distinct niches between interconnected organs. We then introduce the engineering components developed to recapitulate these niches in vitro, most of which were first established in single-organ chips. These toolkits are being adopted in mOoC systems but are not yet fully integrated. Finally, we will summarize how emerging mOoCs deploy these components and discuss future prospects for niche-preserving multi-organ integration.

Preservation of human multi-organ physiological niches

Human organs maintain distinct biochemical microenvironments even as they are interconnected via the vascular network. Each niche exhibits unique spatio–temporal states that reflect differences in growth factor gradients, local cell compositions and extracellular matrix (ECM) architectures. These tissue niches are not preserved in isolation but through the coordinated action of signal buffering, the vascular barrier and organ-specific perfusion.

The liver, for example, produces vascular endothelial growth factor (VEGF) to support its sinusoidal blood vessels[29], yet VEGF signalling remains largely localized to the hepatic environment without triggering vascular remodelling in distant organs (Fig. 2a). This confinement is influenced by ECM composition. Proteoglycans account for approximately 6% of scaffold-associated ECM components[30]. These are dominated by heparan sulfate proteoglycans capable of sequestering the heparin-binding VEGF isoforms VEGF189, VEGF206 and VEGF165 (refs. 31–33). Secreted VEGF binds to these ECM components and signals to adjacent endothelial cells. Free VEGF that enters the bloodstream is buffered by soluble decoy receptors such as sFlt1 (ref. 34). The spatial distribution of growth factors also relies on their inherent molecular properties. Insulin-like growth factor (IGF)-1, which is produced primarily by the liver[35], circulates throughout the body because it does not bind strongly to the liver ECM. Approximately 75–90% of IGFs are carried in ternary complexes with IGF-binding protein (IGFBP)-3 or IGFBP-5 and acid-labile subunit, leaving only a small free fraction in circulation[36,37]. This binding substantially prolongs the half-life of IGF-1 from about 10 min to more than 10 h (ref. 38). IGFBP proteases[39] that are expressed in target organs then cleave IGFBPs to release free IGF-1 into the local microenvironment[39].

In addition to signal buffering, the vascular barrier mediates controlled exchange among multiple organs. The endothelium acts as a selective barrier that regulates molecular passage through tight junctions[40], receptor-mediated transcytosis[41] and the charge-selective glycocalyx[42] (Fig. 2b). Vascular permeability also varies substantially across organs, ranging from fenestrated sinusoids in the liver to continuous capillaries in the heart and skeletal muscle, and the tightly sealed blood–brain barrier[43]. These differences reflect organ-specific endothelial gene expression programs that establish tissue-matched junctional composition, transporters and basement membrane characteristics[44].

Niche preservation also depends on the biomechanical context. In human blood circulation, each organ receives a distinct fraction of cardiac output, with the liver, skeletal muscle and brain receiving approximately 25%, 15% and 12%, respectively[45] (Fig. 2c). This differential perfusion contributes to the local exposure of circulating drugs and signalling molecules[46] such that uniform perfusion across all in vitro compartments cannot reproduce in vivo drug exposure profiles. In addition to flow distribution, capillary flow shear stress is organ-specific, with low shear in hepatic sinusoids[47] and higher shear in pulmonary capillaries[48]. These mechanical inputs can influence substance exchange by regulating the expression of organ-specific transporters and tight junction proteins. Together, signal buffering, the vascular barrier and organ-specific perfusion define human organ niches and shed light on strategies for in vitro recapitulation (Table 1).

Engineering niche-preserving components in single-organ systems

Engineering selective inter-organ exchange requires components that recapitulate each previously identified feature of physiological niche maintenance. Most progress in developing these components stems from single-organ models, which provide the engineering foundation for multi-organ niche integration. These include engineered ECM environments that define biochemical identity within individual niches, passive barriers that separate niches and vascular interfaces that control exchange. We review each component next.

The extracellular matrix as a local signalling niche. The ECM within OoCs can be engineered to achieve controlled cellular interactions and spatial distribution of distinct niches. In native tissues, the ECM acts not only as a dynamic scaffold for cell adhesion but also as a local reservoir for growth factors through reversible non-covalent binding. The affinity can be tuned to modulate growth factor release profiles. For example, synthetic glycosaminoglycans can be systematically screened for their binding kinetics with multiple growth factors. The selected variants can be incorporated into elastin-like recombinamer hydrogels to enable controlled release of fibroblast growth factor 2 and support long-term angiogenesis (Fig. 3a)[49]. Despite advances in ECM engineering, in vitro modelling remains heavily reliant on Matrigel and other native ECM components. Challenges involving complex components, tumorigenic origin, lack of tunability and batch variability limit the biological outcomes and translational potential of Matrigel[50]. These limitations highlight the great potential of tissue-specific engineered ECM with mechanical and chemical tunability.

Signalling molecules themselves can also be engineered to alter their ECM affinity (Fig. 3b). VEGFA and platelet-derived growth factor BB were modified to include heparan sulfate proteoglycan-binding sequences, which produced sustained low-intensity tonic signalling[51]. Clinically approved protein therapeutics can also be modified with a strong ECM-binding motif to greatly extend local retention[52]. In addition to non-covalent strategies, growth factors could be covalently immobilized to biomaterials. For example, sonic hedgehog and ciliary neurotrophic factor can be simultaneously immobilized with 3D precision using two-photon irradiation and orthogonal physical binding pairs[53]. A generalized growth factor immobilization within natural ECM can also be achieved via photomediated oxime ligation. For example, epidermal growth factor can be patterned within collagen gels to control cell proliferation with spatial precision[54]. Bioactive molecules such as Delta-1 can be immobilized in fibrin gels to activate Notch signalling selectively[54].

https://doi.org/10.1038/s41551-026-01806-4

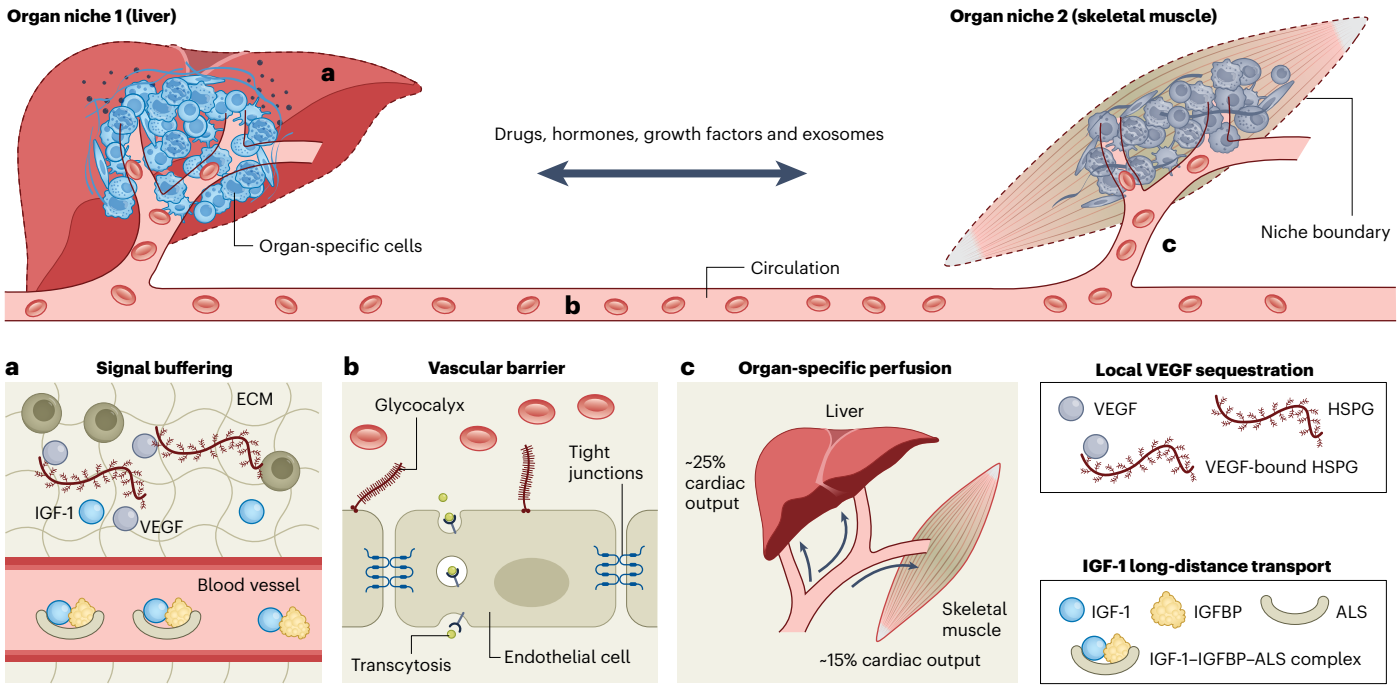


Fig. 2 | Human physiology as a multiniche selective exchange system. Human organs remain interconnected through the systemic circulation while maintaining distinct biochemical microenvironments (red dotted outlines), illustrated here for the liver (organ niche 1) and skeletal muscle (organ niche 2). Drugs, hormones, growth factors and exosomes are exchanged between niches via the bloodstream. **a**, Signal buffering within the tissue niche. Distinct molecules show distinct interaction patterns. Liver-secreted VEGF is largely retained locally by binding cell surface and ECM heparan sulfate proteoglycans (HSPGs). IGF-1, by contrast, enters the bloodstream, where ternary complexes with IGFBPs and the acid-labile subunit (ALS) extend its half-life and enable long-range endocrine signalling. **b**, Selective transport across the endothelium governed by tight junctions, receptor-mediated transcytosis and the charge-selective glycocalyx. **c**, Organ-specific perfusion. Each organ receives a distinct fraction of cardiac output, approximately 25% to the liver and 15% to skeletal muscle, producing organ-specific exposure to circulating molecules. Hepatic flow comprises both arterial and portal inflow.

Passive barriers. Passive barriers refer to structures that provide physical separation and allow diffusion-based transport. Porous membranes are the most common passive barrier between adjacent niches (Fig. 3c). Frequently used membrane materials include polydimethylsiloxane (PDMS)[55], polycarbonate[56], polycaprolactone[57], polyethylene terephthalate[58], polyester[59], silk fibroin[60] and collagen[61]. Pore diameters usually range from 0.4 to 10 µm (ref. 62) and membranes are typically designed to support cell adhesion on one or both sides while preventing whole-cell translocation. Fabrication techniques include replica moulding from photolithography wafers[63,64], laser micromachining[65], in situ crosslinking[66,67] and freeze-drying[61].

A different passive approach is the geometric separation of niches by increasing the diffusion distance through long channels (Fig. 3d). In static cultures and some laminar flow systems, slow Fickian diffusion primarily governs mass transport. If the characteristic diffusion mixing time exceeds the medium replacement interval, each compartment can partially maintain a distinct molecular gradient. This concept has been demonstrated in various gradient-guided differentiation systems. For example, gradients of a fluorescently labelled 70 kDa dextran were stable for up to 72 h in a 150 µm-high microfluidic chip[68]. Using this strategy, spatial morphogen gradients were found to facilitate coordinated co-differentiation of neural tube-like tissue along the rostral–caudal and dorsal–ventral axes[69]. This approach dates back to the Campenot chamber, which created separate compartments connected by narrow low-height microchannels[70]. The same approach is now applied in modern neuron culture chambers and commercial OoC products[71].

Passive barriers facilitate the establishment of cell separation and linear growth factor gradients. However, passive measures are not suitable for establishing a complex pattern that is based on biological identity rather than molecular size.

Vascular interfaces. A common vascularization approach in OoC systems involves forming a confluent endothelial monolayer (Fig. 3e). For example, primary human pulmonary microvascular endothelial cells were co-cultured with airway epithelium to model the viral infection process[72]. Although this design creates a basic vascular interface, the model has limitations in barrier integrity, organ specificity and network complexity. Physiological blood vessels show a wide range of transepithelial electrical resistance (TEER) values—from about 10 $\Omega \cdot cm^2$ in fenestrated capillaries to >1,500 $\Omega \cdot cm^2$ in highly restrictive barriers such as those at the blood–brain interface[73]. By contrast, simplified endothelial monolayers usually reach TEER values of <100 $\Omega \cdot cm^2$ (ref. 74). Creating a more functional vasculature requires the addition of support cells such as pericytes, smooth muscle cells, neurons and fibroblasts, which help maintain endothelial homeostasis[75] and barrier stability[76]. In addition, a uniform, planar endothelial monolayer cannot mimic organ-specific vascular heterogeneity[77,78].

Alternative spontaneous vascularization strategies involve embedding endothelial cells within 3D ECM or inducing them to sprout towards adjacent matrix compartments[79], where they self-organize into interconnected capillary-like networks (Fig. 3f). This angiogenesis-driven vascularization can generate branching lumen structures with more architectural complexity than monolayer or pre-patterned channels. For example, parallel-milled thermoplastic chips with organoid capture structures enable syringe pump perfusion through vascular-like networks at physiologically relevant shear rates[80]. Similarly, a human primary vascularized tumour-on-a-chip system was designed to model chimeric antigen receptor T cell trafficking into tumors through microvasculature[81]. Despite these advances, most studies have focused on vascularizing single organoids in isolation rather than establishing integrated vascular pathways that support communication between multiple organoid niches. In many systems,

Table 1 | Mapping of in vivo niche preservation mechanisms to in vitro engineering components

Mechanism	In vivo basis	In vitro components
Signal buffering	ECM sequestration; plasma protein binding	Engineered ECM and growth factors
Vascular barrier	Endothelial selective barrier; organ-specific permeability	Passive porous membranes; endothelial monolayers; self-assembled vascular networks
Organ-specific perfusion	Differential cardiac output across organs; organ-specific capillary shear stress	Cardiac output-scaled robotic medium transfer; resistance-based distribution

the perfusable microvessels penetrate only shallowly into organoids, making it difficult to sustain tissues larger than the oxygen diffusion limit[82,83]. As for flow, gravity perfusion remains the most widely adopted method[84], although it produces only 1–3 mmHg pressure by the culture media height difference. This is substantially lower than the 10–22.5 mmHg observed in human capillaries[85]. Furthermore, the self-assembled networks resemble only capillaries and not arterioles or venules, limiting the modelling accuracy. Functional pericyte recruitment, basement membrane deposition and lumen stabilization are often incomplete.

Reconstructing multi-organ niches

Emerging mOoC strategies. Based on the niche-preserving components developed in single-niche models, important progress has been made in mOoC niche preservation (Table 2). The simplest architectures couple tissue compartments directly through microchannels or porous membranes. A multi-organoid body-on-a-chip system connected with microchannels demonstrated 28-day viability[86] (Fig. 3g). Scaling this approach with channel dimension matching to in vivo cardiac output, a multilayer 18-organ chip recapitulated organ-specific perfusion volumes and maintained the system for 2 months (ref. 87; Fig. 3h). Rocking-plate tilting-based gravity flow is a widely used perfusion method that enables long-term perfusion without a complex hardware set-up (Fig. 3i). It has been applied to model multi-organ communication[88,89], drug toxicity[90,91], PK and pharmacodynamics (PD)[92]. By tuning channel resistance and topography, rocking-plate platforms can achieve either bidirectional or unidirectional flow[93]. However, these direct medium connection methods may fail to maintain organ-specific media due to cross-compartment mixing, thus eroding phenotypic maturation in long-term culture[27].

This problem can be partly solved by programmable fluidic control. For instance, a gut–liver–brain chip was built to connect three microphysiological systems with pneumatic micropumps for Parkinson's disease modelling using short-chain fatty acid signalling across compartments[26] (Fig. 3j). A robotic liquid handler transferred medium among organ compartments while keeping each in its own tissue-specific culture environment (Fig. 3k). Another study cultured Caco-2 BBe cells, primary human hepatocytes and renal proximal tubule epithelial cells individually in organ-specific media[25]. A robotic liquid transfer from the chip arteriovenous reservoir was then scaled to physiological cardiac output fractions to enable inter-organ communication.

Beyond discrete robotic transfer, an integrated continuous architecture was created using a vascular barrier to physically separate each tissue compartment from a shared vascular flow (Fig. 3l). Using a four-organ heart–liver–bone–skin design, each tissue chamber was found to retain its own optimized medium above a human umbilical vein endothelial cell–mesenchymal stem cell vascular barrier with recirculation flow beneath[27]. Although the vascular interface area was not scaled to match in vivo cardiac output fractions, the system maintained tissue-specific phenotypes for 4 weeks and recapitulated selective $CD14^+$ monocyte enrichment in injured cardiac tissue. Notably, despite identical initial vascular conditions across all organ compartments, liver-adjacent endothelial cells spontaneously exhibited reduced VE-cadherin expression and lower TEER values[27]. Although this endothelium was not characterized further for sinusoidal identity, these results highlighted the importance of niche preservation across organs.

In addition to barrier engineering, recent advances have incorporated tissue-specific ECM and oxygen environments. One study featured a heart–liver–bone–skin-on-a-chip that used fibrin for heart and liver, decellularized bovine bone scaffold for bone and collagen for skin[27]. A six-organoid screening system used rat tail collagen I for liver organoids and solubilized human testis ECM for the testis compartments[86]. A mOoC design introduced organ-specific oxygen tensions of 13%, 5% and 13% for liver, kidney and arterial vessel, respectively[94]. Under acetaminophen exposure, this system revealed that oxygen tension modulates both drug toxicity and metabolic activity.

Further engineering innovations have enabled mOoCs to quantitatively predict human PK and PD, supporting mOoC translational value in drug development. The arteriovenous reservoir gut–liver–kidney platform and bone marrow–liver–kidney platform quantitatively predicted human PK responses for nicotine and cisplatin across multiple dosing regimens using computational physiologically based PK model data that were validated against clinical reference data[25]. The cisplatin model also recapitulated bone marrow toxicity as a PD end point[25]. A companion robotic interrogator study extended to eight organ chips to validate the multicompartmental reduced-order PK model[95]. The heart–liver–bone–skin chip recapitulated the clinical PK profile of doxorubicin and identified miR-1 as an early cardiotoxicity biomarker, consistent with both paediatric and adult clinical signatures[27]. The 18-organ chip reproduced the two-compartment PK of carboplatin with a half-life of 1.34 h, achieving in vitro reproduction of two-compartment drug time curves[87].

Limitations of emerging mOoC strategies. Although existing mOoC systems can maintain tissue-specific media, impose organ-relevant oxygen concentrations, scale inter-organ flow to cardiac output fractions, incorporate vascular barriers and generate spontaneous microvascular networks, these advances remain fragmented. No platform has yet integrated these features into a fully physiologically 3D multi-organ architecture. A central challenge is the construction of functional perfusable vascular networks not only within individual niches but also connecting niches through hierarchical arteriole–capillary–venule structures. Proof-of-concept studies show that vascular networks formed in adjacent compartments can merge and become perfusable[80,96] but robust arteriole and venule self-organization remains unresolved. Tissue-specific ECM reconstruction is also incomplete. Many platforms rely on broadly permissive matrices such as Matrigel, collagen, fibrin or decellularized ECM[27,81]. These materials support tissue formation but only partially recapitulate the biochemical composition[97,98] and viscoelastic[99] heterogeneity of native organ ECM.

A second major challenge is reproducibility and standardization. Many mOoCs are fabricated using laboratory-scale methods such as PDMS moulding and manual assembly, which can introduce variation in geometry, flow resistance and surface properties. Across laboratories, mOoC designs also vary by layout, tissue scaling, fluidic routing, vascular interface and medium composition, making cross-study comparisons even more difficult. Standardized modular design, reliable flow systems and quantitative quality control metrics would be essential for translating mOoCs beyond laboratory prototypes. Readout capacity imposes another bottleneck. End point assays, destructive extraction and off-chip sampling greatly restrict the throughput. Integration of non-invasive multimodal readouts would substantially increase the information content of mOoCs and strengthen their utility for biological evaluation and drug response prediction.

https://doi.org/10.1038/s41551-026-01806-4

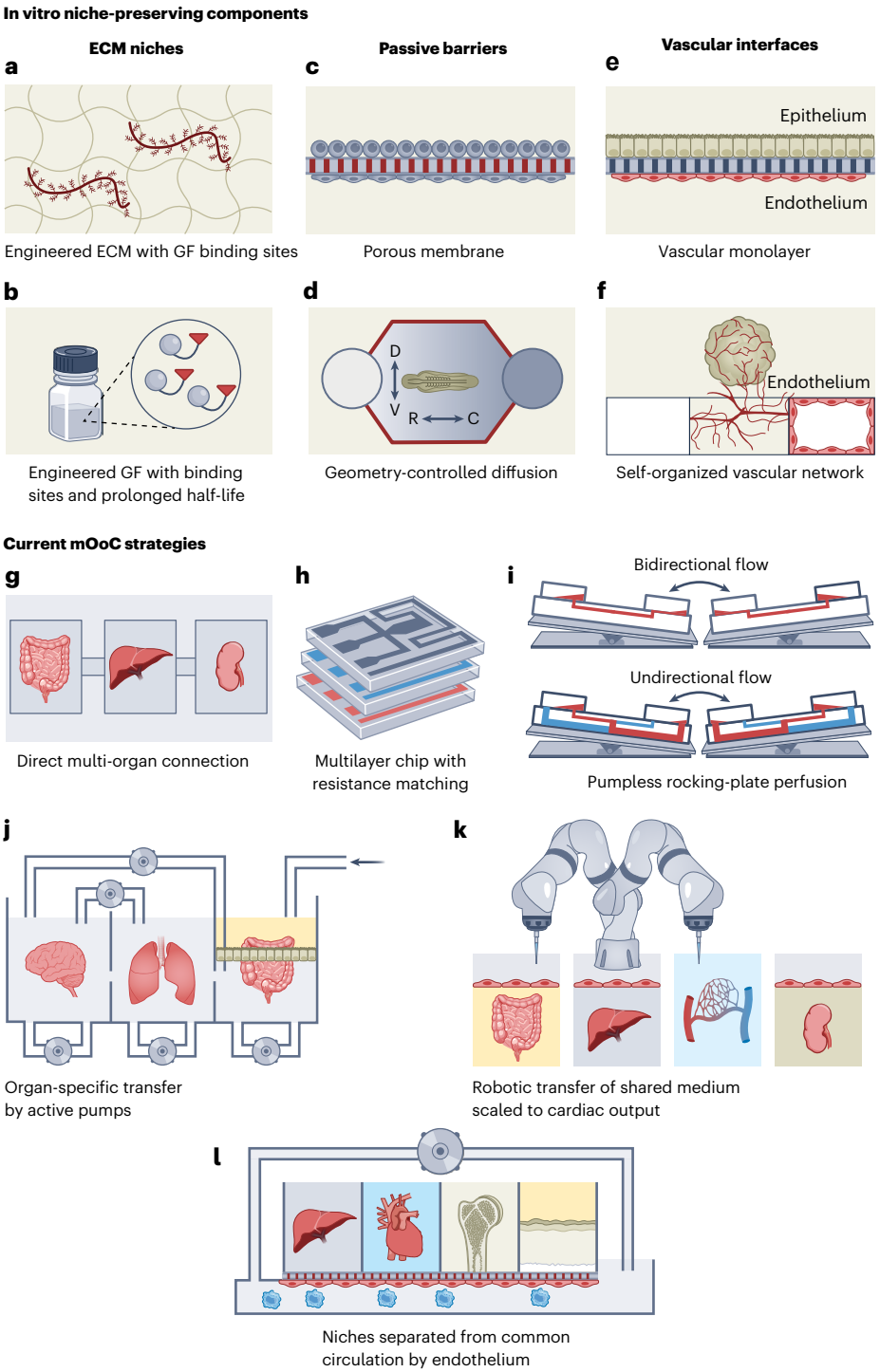


Fig. 3 | Engineering niche-preserving components and emerging mOoC strategies. a–**f**, Engineering niche-preserving components developed from single-organ models. **a**,**b**, Extracellular matrix (**a**) and growth factors (GFs; **b**) can be engineered with binding motifs to sequester and localize signals. **c**,**d**, Advances in microenvironmental barrier engineering include porous membranes that prevent cell mixing (**c**) and geometric separation that enables linear GF gradients for patterned neural tube differentiation (**d**). C, caudal axis; D, dorsal axis; R, rostral axis; V, ventral axis. **e**,**f**, Vascular barriers include single-layer endothelium (**e**) and spontaneous vascular networks to support molecular exchange (**f**). Capillary models are the most established vascular-on-chip systems. **g**–**l**, mOoC strategies available at present. **g**, Direct connection of multi-organ compartments through microchannels. **h**, Multilayer microfluidic chip assembly that models the arteriovenous vascular network in the human body, with flow resistance to each organ scaled to resting-state cardiac output. **i**, Pumpless rocking-plate perfusion. Gravity-driven flow by chip tilting enables inter-organ communications. Bidirectional and unidirectional flow can be achieved through channel resistance and topography design. **j**, Multi-organ assembly with passive flow, active pumping perfusion and intra-niche recirculation circuit. **k**, Lung, liver and kidney organ chips with individual culture media in the organ compartment. The robotic liquid handler transfers shared medium from the vascular side at flow rates scaled to cardiac output. **l**, Endothelium-separated multi-organ niches sharing a common circulation with immune cells.

Towards standardized data-rich new approach methodologies

Scalable manufacturing for mOoC platforms

Niche-preserving mOoC architectures pose manufacturing challenges that extend beyond general microfluidic fabrication. A single mOoC device should integrate organ-specific tissue chambers, vascular barriers and circulation channels. Chip materials should also minimize small-molecule absorption to maintain inter-organ culture conditions and drug concentrations over time. Scalable fabrication and standardized modular assembly are also needed to improve the robustness and translation capabilities of multi-organ models.

Photolithography-based PDMS casting is the classical method for mOoC fabrication[25,95]. Despite its high channel precision and optical transparency, PDMS can substantially absorb hydrophobic small molecules both at the surface and within the bulk material[100]. This absorption is particularly problematic for multi-organ models as it compromises the distinct drug concentrations in each organ compartment and undermines subsequent PK–PD prediction. The clean room facility requirements and time-consuming master fabrication further limit the rapid design iteration. Additive manufacturing approaches such as stereolithography and its projection-based variants[101–103] enable flexible ultraviolet curing of photosensitive resin to fabricate irregular mOoC compartment geometries[104]. However, challenges such as resin biocompatibility, surface roughness, optical transparency and mechanical properties remain. For multilayer mOoC assembly designs, laser patterning of polymethyl methacrylate is often adopted[86,87,94]. Computer numerical control milling of thermoplastics such as polysulfone has also been used for mOoC part fabrication[27]. For scale-up production, injection moulding of thermoplastic replicates enables high-precision large-scale production of mOoC devices[105]; however, high tooling costs limit industrial-scale production.

Beyond specific fabrication methods, mOoC manufacturing is shifting from dedicated single-purpose chips towards modular plug-and-play platforms with standardized components. The four-OoC platform uses a universal stand with interchangeable tissue inserts, allowing the same system to be reconfigured across organ combinations and reused for other applications[27]. Pumping architectures show a similar trend. Multi-organ platforms increasingly adopt easy-to-use pumping strategies that scale across parallel devices, including peristaltic pumps for medium recirculation[27], impeller modules that drive multiple chips in parallel[104,106] and on-chip geometry-based pumps that control flow through integrated microvalves and capacitors[107,108]. Modular designs, standardized interfaces and accessible pumping systems represent an emerging direction in mOoC manufacturing aimed at simplifying adoption by biologists without expertise in chip fabrication or fluidic engineering.

Multimodal readouts for drug effect characterization

Current mOoC readouts for drug response analysis typically include medium sampling, tissue retrieval, end point staining, biochemical assays, mass spectrometry analysis and computational reconstruction[25,27,87]. Although these methods have enabled PK–PD and toxicity demonstrations, they provide limited longitudinal information and often require off-chip or destructive analysis. As a result, it remains difficult to continuously resolve how each organ compartment responds to drug exposure over time. Realizing the translational value of niche-preserving mOoCs will require multimodal readouts that can quantify drug effects non-invasively across multiple compartments and throughout the full exposure period. We therefore next review the principal readout modalities: biological assays, optical imaging, and electrical, mechanical and chemical sensing. Many of the approaches discussed below were originally developed for organoids, engineered tissues or single OoCs and were subsequently adapted to mOoC systems. Nevertheless, the device settings and data modalities provide transferable strategies for future mOoC readout integration.

Biological readouts. Biological readouts remain the foundation for assessing drug-induced effects (Fig. 4a). In addition to traditional methods such as immunostaining and western blotting, multi-omics platforms now generate much larger human-relevant datasets for targeted drug discovery and development. Active reinforcement learning frameworks have been applied to single-cell transcriptomics to guide phenotypic drug screening[109]. Spatial transcriptomics has uncovered coordination of immune cell polarity, as exemplified by CXCL16–SPP1 macrophage states[110]. Chemical proteomics has mapped the target landscape of 1,000 kinase inhibitors, providing broad insights into drug–protein interactions[111]. Metabolomics has been used to identify enzyme targets of small molecules[112]. Although multi-omics predictions often require further experimental validation, multi-omics-driven drug development is becoming a necessary precursor. Algorithms capable of handling large volumes of data and the integration of multiple data types will be crucial for extracting meaningful biological insights.

Optical readouts. Optical imaging is a vital data modality because it enables cost-effective, non-invasive and high-throughput analysis of biological samples (Fig. 4b). Bright-field microscopy remains the standard approach for routine observation and quality control. Fluorescence-based techniques, such as confocal microscopy and light-sheet microscopy, serve as the primary tools for target-specific imaging, providing molecular specificity and 3D spatial resolution; however, their imaging depth is typically limited to 100–150 µm. For organoids, such as cerebral organoids that are several hundred micrometres in diameter, optical clearing is often necessary to match the refractive index and enable deep tissue visualization[113].

Despite high imaging quality, fluorescence microscopy is limited by a small field of view and long acquisition times. High-content imaging methods partly address these issues through automated stage movement and image stitching, but the process remains time-consuming. Multi-scale and high-throughput imaging is emerging as a promising approach. For example, microfabricated organoid culture and imaging chips such as the JeWell system have shown promising results[114]. Featuring thousands of pyramidal wells flanked by 45° mirrors, JeWell supports selective plane illumination microscopy and is compatible with standard commercial fluorescence microscopes. When paired with a laser-steering unit, JeWell chips enable light-sheet imaging of up to 300 organoids per hour at subcellular resolution[114].

Several emerging modalities are being developed to achieve label-free optical imaging with higher speed and greater depth. Label-free methods are particularly well suited to time-lapse imaging of culture dynamics. Holotomography is a 3D refractive index-based technique that enables long-term, label-free imaging of spheroids and organoids at subcellular resolution without photobleaching[115]. However, its imaging depth is typically constrained to <150 µm (ref. 116). Photoacoustic imaging detects ultrasound signals generated by tissue under pulsed laser excitation[117]. Because acoustic waves scatter less than photons, photoacoustic imaging enables live tissue imaging for applications such as breast cancer detection[118], lymphatic vessel visualization[119] and blood vessel imaging[120]. Recent progress in volumetric photoacoustic imaging permits the imaging of human brain organoids at depths of about 500 µm with a lateral resolution of around 2 µm (ref. 121). Metalens-based designs have expanded the optical depth of field, enabling single-scan imaging throughout the entire organoid, regardless of thickness. Computational imaging algorithms then reconstruct images at various depths, significantly reducing imaging time[121]. Optical coherence tomography (OCT) uses low-coherence near-infra-red light and interferometry to acquire depth-resolved signals. Full-field OCT can reach millimetre-scale depths, with an axial resolution of 1.7 µm and a lateral resolution of 0.5 µm, in retinal organoid imaging[122]. Future research should continue exploring label-free imaging methods with greater penetration depths. Training models

https://doi.org/10.1038/s41551-026-01806-4

Table 2 | Representative works on mOoC devices

Study	Number of organ compartments	Tissue source	Circulation architecture	Organ-specific ECM niche	Organ-specific media	Organ-specific oxygen	Endothelialized vasculature	Organ-specific perfusion	Culture duration	Drug response demonstration
Miller and Shuler[88]	13: skin, gastrointestinal tract, lung, fat, kidney, heart, adrenal gland, liver, spleen, brain, pancreas, bone marrow, muscle	Human cell lines (A549, Caco-2, HepG2 C3A, Meg01 and HK2)	Pumpless rocking-plate perfusion	No. PGMatrix	No	No	No	Yes	7 d	NA
Oleaga et al.[90]	4: liver, heart, skeletal muscle, neuron	Primary cells, hiPSC and cell lines	Pumpless rocking-plate perfusion	No. Collagen, fibronectin, DETA, laminin coating	No	No	No	No	14 d	Doxorubicin, atorvastatin, valproic acid, acetaminophen, AMAP
Novak et al.[95]	8: gut, liver, kidney, heart, lung, skin, BBB, brain	Primary cells, hiPSC and cell lines	Robotic medium transfer	No. Collagen and fibronectin coating	Yes	No	Yes. Within each chip	No	3 weeks	Inulin–FITC tracer PK
Herland et al.[25]	3: gut–liver–kidney; bone marrow–liver–kidney	Primary hepatocytes, RPTECs, $CD34^+$ progenitors and Caco-2 cells	Robotic medium transfer	No. Fibronectin, collagen, laminin, Matrigel coating	Yes	No	Yes. Within each chip	Yes	10 d	Quantitative PK for nicotine and PK–PD for cisplatin
Skardal et al.[86]	6: liver, heart, lung, vessel, testis, and colon or brain	Primary cells, hiPSC and cell lines	Micro-peristaltic pump	Partial. Decellularized human organ-specific ECM for lung and testis. Non-specific ECM for other organs	No	No	Partial	No	28 d	Drug screening and toxicity demonstration
Trapecar et al.[26]	3: gut–liver–brain and circulating immune cells	Primary cells and hiPSC-differentiated cells	On-board pneumatic micropumps	No. Collagen	Partial	No	No	Partial	4 d	NA
Ronaldson-Bouchard et al.[27]	4: heart, liver, bone, skin	hiPSC-derived cardiac, hepatic or bone tissues; primary cells	Peristaltic pump	Yes. Fibrin (heart, liver), bovine bone scaffold (bone), collagen (skin)	Yes	No	Yes. HUVEC–MSC layer	No	4 weeks	Doxorubicin PK–PD, cardiotoxicity microRNA
Jiang et al.[94]	3 parallel: liver, kidney, vessel	Cell lines	Peristaltic pump	No. GelMA	No	Yes	No	No	7 d	Acetaminophen toxicity, oxygen-dependent drug response
Wang et al.[87]	18 rat organs such as brain, heart, lung, liver and so on	Fresh rat microtissues; native tumour tissue	Peristaltic pump	Partial. Native ECM	Partial	No	No	Yes	2 months	Carboplatin PK–PD and toxicity
Cook et al.[104]	2–4: lymph node with upstream injection or tissue site	Murine lymph node tissue slices	Magnetic impeller pump	Partial. Native ECM	No	No	No	No	24 h	NA

AMAP, 3-acetamidophenol; BBB, blood–brain barrier; DETA, *N*-1(3-(trimethoxysilyl)propyl)diethylenetriamine; FITC, fluorescein isothiocyanate; GelMA, gelatin methacryloyl; hiPSC, human induced pluripotent stem cell; HUVEC, human umbilical vein endothelial cell; MSC, mesenchymal stem cell; NA, not applicable; RPTEC, renal proximal tubule epithelial cell.

https://doi.org/10.1038/s41551-026-01806-4

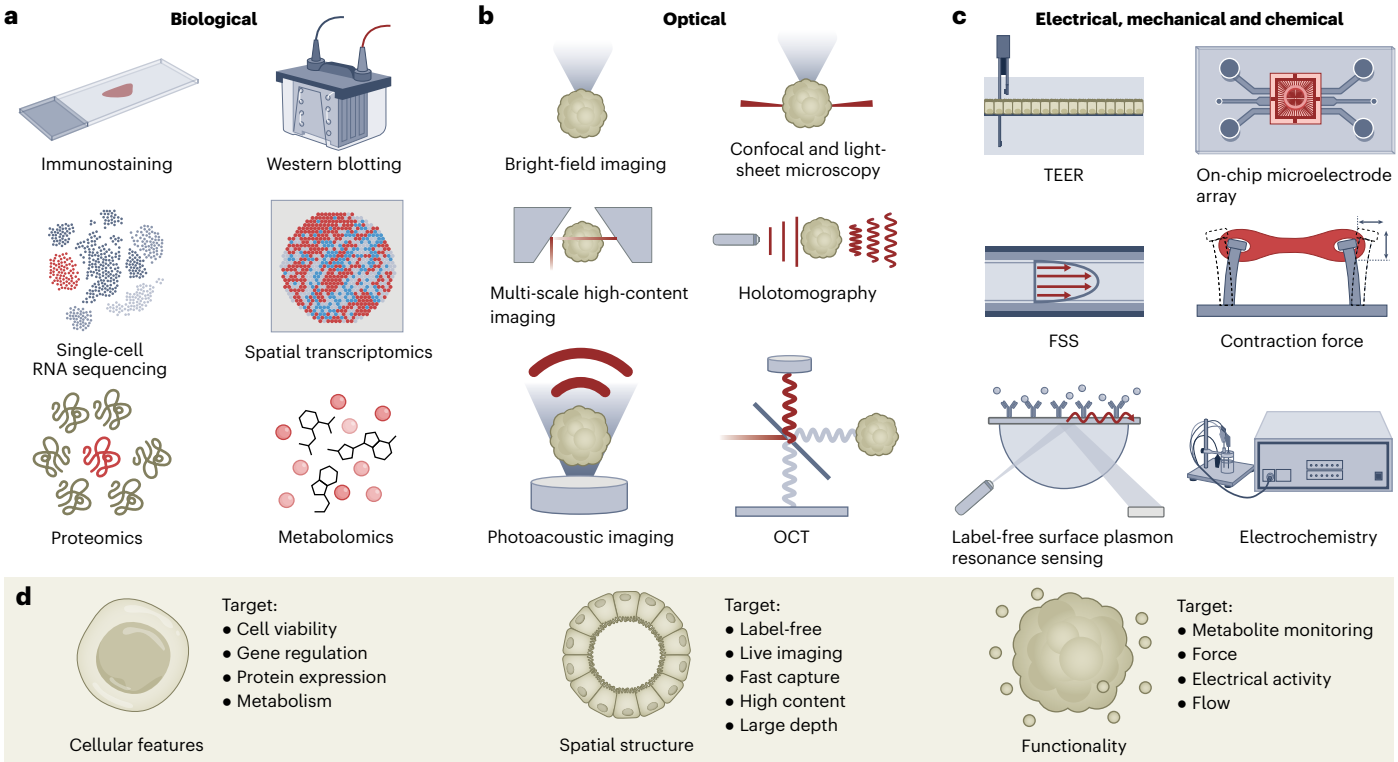


Fig. 4 | Integration of multimodal readouts from new approach methodologies for comprehensive drug evaluation. a, Biological readouts. Immunostaining, western blotting and multi-omics analyses reveal drug-induced biological changes. **b**, Optical readouts. Image-based measurements remain the most powerful readouts in NAMs. Bright-field imaging; fluorescence-based methods such as confocal microscopy, light-sheet microscopy and multi-scale high-content imaging; and label-free modalities such as holotomography, photoacoustic imaging and OCT provide access to drug-induced changes in 3D organoid structure and morphology at large imaging depths. **c**, Electrical, mechanical and chemical readouts. Transepithelial electrical resistance, on-chip microelectrode array recordings, FSS sensing, contraction force measurements, surface plasmon resonance and electrochemistry capture functional responses to drug exposure and characterize the physiological performance of the on-chip models. **d**, Together, these orthogonal structural, functional and molecular readouts provide an in-depth multimodal framework for drug development and evaluation using in vitro NAM systems.

using fluorescence imaging data as ground truth to align signals with label-free or bright-field images could greatly improve the characterization of in vitro NAMs.

Electrical, mechanical and chemical readouts. In addition to optical readouts, a thorough evaluation of drug-induced biological effects requires functional characterization, including electrical, mechanical and chemical signals (Fig. 4c). TEER is a common method for assessing cell layer integrity and barrier function, frequently serving as a predictive indicator of drug-induced toxicity. For example, TEER measurements using confluent layers derived from primary intestinal stem cells were used to predict drug-induced diarrhoea risk[123]. In addition to average impedance values, high-density microelectrode arrays enable spatial impedance mapping at single-cell resolution[124]. Microelectrode arrays can also be combined with microfluidic chips to monitor neuronal activity[125], providing real-time insights into tissue-level function.

Next, mechanical readouts are crucial for characterizing flow dynamics and contractile behaviour in OoC systems. Given that most OoCs involve perfusion, assessment of fluid shear stress (FSS) is essential. However, direct measurement of FSS is difficult. In vivo, near-wall flow velocity is usually estimated using Doppler ultrasound or magnetic resonance imaging. On-chip FSS can be inferred through computational fluid dynamics based on channel geometry or measured using cell-based sensors[126] and microparticle velocimetry[80]. In addition to flow, cellular force generation is an essential functional indicator. In one common strategy, cellular forces can be inferred by imaging the movement of embedded microparticles in traction force microscopy[127]. Alternatively, the movement of microcantilevers with integrated electrodes converts contraction-induced mechanical deformation into electrical signals, enabling electromechanical testing of drug toxicity in cardiac models[128].

Two-post tissue engineering methods, such as those used for engineered heart tissue, are the most common systems for measuring microtissue contractile force by translating tissue contraction into post deflection[129]. However, the force measurement varies with the location of the engineered heart tissue on the post and is incompatible with 3D organoids due to the spherical shape and size. Although image-based tools such as MuscleMotion[130] can track pixel displacement and deformation over time, they cannot map to absolute force values with fidelity. The development of reliable force quantification methods compatible with organoid and OoC systems will be essential for advancing mechanical readouts in drug compound screening.

Finally, chemical modalities have shown promise for detecting metabolites. Nanoplasmonic biosensors[131] can detect drug-induced changes in VEGFA secretion with spatial and temporal resolution, allowing real-time evaluation of drug effects on secretion dynamics[132,133]. Single-walled carbon nanotube electrochemical sensors have also been used to specifically detect dopamine and serotonin release at nanomolar concentrations in real time[134]. Combining chemical content imaging with biological imaging offers great potential for in situ monitoring of both molecular and structural dynamics. Hyperspectral, nonlinear optical methods (such as coherent anti-Stokes Raman scattering microscopy) offer a label-free strategy to assess not only the tissue structure but also the chemical nature of the sample[135–137]. In summary, electrical, mechanical and chemical measurements provide essential functional readouts of NAMs, and integrating all three will be vital for advancing comprehensive NAM-based characterization, target drug screening and lead compound assessment (Fig. 4d).

Future outlook

Over the past two decades, the use of NAMs has advanced in vitro mOoC engineering and high-content data output such as label-free in situ detection. Aided by the expansion of human-relevant datasets and the regulatory momentum from the FDA Modernization Act 3.0, NAMs show growing promise in translational potential and impact. Future progress will depend on the integration of niche-preserving mOoC engineering, scalable manufacturing and multimodal readouts into coherent platforms.

A central focus is to develop mOoC systems with specialized niches and regulated communication between them. By viewing human physiology as a coordinated network of selective microenvironments rather than as isolated units, NAMs can better replicate human ADMET processes compared with conventional approaches. Vascularized structures that maintain niches and enable adjustable molecular exchange can improve the physiological relevance of in vitro pharmacological testing. The implementation of NAMs also depends on scalable and accessible manufacturing. Moving from custom research-grade devices to modular scalable platforms will be crucial for industrial adoption and regulatory approval. As mOoC technologies scale, their utility will increasingly depend on multimodal high-content readouts that combine label-free computational imaging, functional sensing and multi-omics, paired with standardized pipelines for data processing and reporting.

These engineering advances together may enable a future in which mOoCs will serve as a key experimental substrate for artificial intelligence (AI)-driven drug discovery. Current AI applications in NAM contexts have been demonstrated principally at the single-organ level rather than at the mOoC scale. Bright-field liver organoid images trained with deep learning models predicted liver toxicity of FDA-approved drugs with 82% accuracy[138]. LabelFreeTracker used confocal fluorescence images of intestinal organoids to train a U-Net network capable of predicting nuclear and membrane features from bright-field images[139]. Paired bright-field and live–dead-stained images have been trained with large-model-based algorithms to realize virtual viability staining for drug efficacy evaluation[140]. Models trained on pluripotent stem cell morphology in bright-field images can predict differentiation stages and reduce variability across batches[141]. Deep learning has been used to infer retina and anterior neural fold homeobox (RAX) expression and developmental outcomes of hypothalamic–pituitary organoids from early morphological features[142]. These single-organoid demonstrations establish the feasibility of AI-based analysis of NAM imaging data and provide a precedent for future mOoC–AI integrated systems. Scaling these approaches to mOoC platforms will require the niche-preserving architectures, reproducible manufacturing and multimodal readouts developed in the preceding sections together with sustained accumulation of standardized on-chip datasets that AI models can train on. As these substrates mature, mOoCs may evolve from standalone drug evaluation platforms into iteratively improving components of data-driven, human-relevant drug discovery.

References

1. Atkins, J. T. et al. Pre-clinical animal models are poor predictors of human toxicities in phase 1 oncology clinical trials. *Br. J. Cancer* **123**, 1496–1501 (2020).
2. Basit, A. et al. Comparison of tissue abundance of non-cytochrome P450 drug-metabolizing enzymes by quantitative proteomics between humans and laboratory animal species. *Drug Metab. Dispos.* **50**, 197–203 (2022).
3. Fisher, E. M. C. & Bannerman, D. M. Mouse models of neurodegeneration: know your question, know your mouse. *Sci. Transl. Med.* **11**, eaaq1818 (2019).
4. Masubuchi, T. et al. Functional differences between rodent and human PD-1 linked to evolutionary divergence. *Sci. Immunol.* **10**, eads6295 (2025).
5. Eastwood, D. et al. Monoclonal antibody TGN1412 trial failure explained by species differences in CD28 expression on $CD4^+$ effector memory T-cells. *Br. J. Pharmacol.* **161**, 512–526 (2010).
6. Ingber, D. E. Challenges and opportunities for human organ chips in FDA assessments and pharma pipelines. *Cell Stem Cell* **33**, 176–183 (2026).
7. Liu, W., Pang, P. D., Wu, C. A., Tagle, D. & Wu, J. C. New approach methodologies for drug discovery. *Cell* **189**, 1877–1903 (2026).
8. Wu, X., Wu, M. A., Zou, J., Kleinstreuer, N. & Wu, J. C. Reimagining human-centric drug development with new approach methodologies. *Science* **392**, 371–378 (2026).
9. Herron, T. J. et al. Alternatives to animal testing are the future — it's time that journals, funders and scientists embrace them. *Nature* **646**, 799–801 (2025).
10. US Food and Drug Administration. New Approach Methodologies (NAMs). *FDA* https://go.nature.com/3SEpg3o (2026).
11. National Institutes of Health. NIH to prioritize human-based research technologies. *NIH* https://go.nature.com/4A87sys (29 April 2025).
12. Gramm, D. Political appointee tells CDC to end monkey research. *Science* **390**, 868–869 https://doi.org/10.1126/science.zd25zhr (2025).
13. Hong, D.-y. K-Organoid Consortium launches to advance organoid research and replace animal testing. *ChosunBiz* https://go.nature.com/4ip9rYR (14 August 2025).
14. Zhang, S. Y., Ong, W. S. Y., Subelzu, N. & Gleeson, J. P. Validation of a Caco-2 microfluidic chip model for predicting intestinal absorption of BCS class I–IV drugs. *Int. J. Pharm.* **656**, 124089 (2024).
15. Lester, R. M. Update on ICH E14/S7B cardiac safety regulations: the expanded role of preclinical assays and the "double-negative" scenario. *Clin. Pharmacol. Drug Dev.* **10**, 964–973 (2021).
16. Abilez, O. J. et al. Gastruloids enable modeling of the earliest stages of human cardiac and hepatic vascularization. *Science* **388**, eadu9375 (2025).
17. Wang, H.-M. et al. Using patient-derived organoids to predict locally advanced or metastatic lung cancer tumor response: a real-world study. *Cell Rep. Med.* **4**, 100911 (2023).
18. Zhao, Y. et al. Integrating organoids and organ-on-a-chip devices. *Nat. Rev. Bioeng.* **2**, 588–608 (2024).
19. Lorenzo-Martín, L. F. et al. Spatiotemporally resolved colorectal oncogenesis in mini-colons ex vivo. *Nature* **629**, 450–457 (2024).
20. Zimmermann, M., Zimmermann-Kogadeeva, M., Wegmann, R. & Goodman, A. L. Mapping human microbiome drug metabolism by gut bacteria and their genes. *Nature* **570**, 462–467 (2019).
21. Guengerich, F. P. Inhibition of cytochrome P450 enzymes by drugs—molecular basis and practical applications. *Biomol. Ther.* **30**, 1–18 (2022).
22. Duregotti, E. et al. Reduced secretion of neuronal growth regulator 1 contributes to impaired adipose-neuronal crosstalk in obesity. *Nat. Commun.* **13**, 7269 (2022).
23. Kim, J. et al. Human assembloid model of the ascending neural sensory pathway. *Nature* **642**, 143–153 (2025).
24. Edington, C. D. et al. Interconnected microphysiological systems for quantitative biology and pharmacology studies. *Sci. Rep.* **8**, 4530 (2018).
25. Herland, A. et al. Quantitative prediction of human pharmacokinetic responses to drugs via fluidically coupled vascularized organ chips. *Nat. Biomed. Eng.* **4**, 421–436 (2020).
26. Trapecar, M. et al. Human physiomimetic model integrating microphysiological systems of the gut, liver, and brain for studies of neurodegenerative diseases. *Sci. Adv.* **7**, eabd1707 (2021).
27. Ronaldson-Bouchard, K. et al. A multi-organ chip with matured tissue niches linked by vascular flow. *Nat. Biomed. Eng.* **6**, 351–371 (2022).

28. Lieleg, O. & Ribbeck, K. Biological hydrogels as selective diffusion barriers. *Trends Cell Biol.* **21**, 543–551 (2011).
29. Mariotti, V., Fiorotto, R., Cadamuro, M., Fabris, L. & Strazzabosco, M. New insights on the role of vascular endothelial growth factor in biliary pathophysiology. *JHEP Rep.* **3**, 100251 (2021).
30. Baiocchini, A. et al. Extracellular matrix molecular remodeling in human liver fibrosis evolution. *PLoS ONE* **11**, e0151736 (2016).
31. Häcker, U., Nybakken, K. & Perrimon, N. Heparan sulphate proteoglycans: the sweet side of development. *Nat. Rev. Mol. Cell Biol.* **6**, 530–541 (2005).
32. Park, J. E., Keller, G.-A. & Ferrara, N. The vascular endothelial growth factor (VEGF) isoforms: differential deposition into the subepithelial extracellular matrix and bioactivity of extracellular matrix-bound VEGF. *Mol. Biol. Cell* **4**, 1317–1326 (1993).
33. Houck, K. A., Leung, D. W., Rowland, A. M., Winer, J. & Ferrara, N. Dual regulation of vascular endothelial growth factor bioavailability by genetic and proteolytic mechanisms. *J. Biol. Chem.* **267**, 26031–26037 (1992).
34. Tang, Y. et al. VEGF and sFLT-1 in serum of PIH patients and effects on the foetus. *Exp. Ther. Med.* **17**, 2123–2128 (2019).
35. Ohlsson, C. et al. The role of liver-derived insulin-like growth factor-I. *Endocr. Rev.* **30**, 494–535 (2009).
36. Bach, L. A. 40 years of IGF1: IGF-binding proteins. *J. Mol. Endocrinol.* **61**, T11–T28 (2018).
37. Kim, H. et al. Structural basis for assembly and disassembly of the IGF/IGFBP/ALS ternary complex. *Nat. Commun.* **13**, 4434 (2022).
38. Forbes, B., McCarthy, P. & Norton, R. Insulin-like growth factor binding proteins: a structural perspective. *Front. Endocrinol.* **3**, 38 (2012).
39. Andrew, M. et al. PAPPA2 as a therapeutic modulator of IGF-I bioavailability: in vivo and in vitro evidence. *J. Endocr. Soc.* **2**, 646–656 (2018).
40. Cong, X. & Kong, W. Endothelial tight junctions and their regulatory signaling pathways in vascular homeostasis and disease. *Cell. Signal.* **66**, 109485 (2020).
41. Baghirov, H. Mechanisms of receptor-mediated transcytosis at the blood–brain barrier. *J. Control. Release* **381**, 113595 (2025).
42. Moore, K. H., Murphy, H. A. & George, E. M. The glycocalyx: a central regulator of vascular function. *Am. J. Physiol. Regul. Integr. Comp. Physiol.* **320**, R508–R518 (2021).
43. Augustin, H. G. & Koh, G. Y. Organotypic vasculature: from descriptive heterogeneity to functional pathophysiology. *Science* **357**, eaal2379 (2017).
44. Trimm, E. & Red-Horse, K. Vascular endothelial cell development and diversity. *Nat. Rev. Cardiol.* **20**, 197–210 (2023).
45. Williams, L. R. & Leggett, R. W. Reference values for resting blood flow to organs of man. *Clin. Phys. Physiol. Meas.* **10**, 187–217 (1989).
46. Fagiolino, P. The influence of cardiac output distribution on the tissue/plasma drug concentration ratio. *Eur. J. Drug Metab. Pharmacokinet.* **27**, 79–81 (2002).
47. Trevisan, B. et al. Effects of shear stress on production of FVIII and vWF in a cell-based therapeutic for hemophilia A. *Front. Bioeng. Biotechnol.* **9**, 639070 (2021).
48. Lin, C. et al. Mechanotransduction regulates the interplays between alveolar epithelial and vascular endothelial cells in lung. *Front. Physiol.* **13**, 818394 (2022).
49. Söderlund, Z. et al. Controlled release of growth factors using synthetic glycosaminoglycans in a modular macroporous scaffold for tissue regeneration. *Commun. Biol.* **5**, 1349 (2022).
50. Wolff, L. & Hendrix, S. Rethinking Matrigel: the complex journey to matrix alternatives in organoid culture. *Adv. Sci.* **12**, e08734 (2025).
51. Mochizuki, M. et al. Growth factors with enhanced syndecan binding generate tonic signalling and promote tissue healing. *Nat. Biomed. Eng.* **4**, 463–475 (2020).
52. Alshoubaki, Y. K. et al. A superior extracellular matrix binding motif to enhance the regenerative activity and safety of therapeutic proteins. *npj Regen. Med.* **8**, 25 (2023).
53. Wylie, R. G. et al. Spatially controlled simultaneous patterning of multiple growth factors in three-dimensional hydrogels. *Nat. Mater.* **10**, 799–806 (2011).
54. Batalov, I., Stevens, K. R. & DeForest, C. A. Photopatterned biomolecule immobilization to guide three-dimensional cell fate in natural protein-based hydrogels. *Proc. Natl Acad. Sci. USA* **118**, e2014194118 (2021).
55. Xie, Y. et al. A flexible strategy to fabricate trumpet-shaped porous PDMS membranes for organ-on-chip application. *Biomicrofluidics* **18**, 054101 (2024).
56. Shah, P. et al. A microfluidics-based in vitro model of the gastrointestinal human–microbe interface. *Nat. Commun.* **7**, 11535 (2016).
57. Kim, D., Lim, H., Youn, J., Park, T.-E. & Kim, D. S. Scalable production of uniform and mature organoids in a 3D geometrically-engineered permeable membrane. *Nat. Commun.* **15**, 9420 (2024).
58. Maurer, M. et al. A three-dimensional immunocompetent intestine-on-chip model as in vitro platform for functional and microbial interaction studies. *Biomaterials* **220**, 119396 (2019).
59. Byrne, C. E. et al. Adaptable manufacturing and biofabrication of milliscale organ chips with perfusable vascular beds. *Biotechnol. J.* **19**, e202400550 (2024).
60. Mou, X., Shah, J., Roye, Y., Du, C. & Musah, S. An ultrathin membrane mediates tissue-specific morphogenesis and barrier function in a human kidney chip. *Sci. Adv.* **10**, eadn2689 (2024).
61. Wang, C., Tanataweethum, N., Karnik, S. & Bhushan, A. Novel microfluidic colon with an extracellular matrix membrane. *ACS Biomater. Sci. Eng.* **4**, 1377–1385 (2018).
62. Corral-Nájera, K., Chauhan, G., Serna-Saldívar, S. O., Martínez-Chapa, S. O. & Aeinehvand, M. M. Polymeric and biological membranes for organ-on-a-chip devices. *Microsyst. Nanoeng.* **9**, 107 (2023).
63. Huh, D. et al. Reconstituting organ-level lung functions on a chip. *Science* **328**, 1662–1668 (2010).
64. Kim, H. J., Huh, D., Hamilton, G. & Ingber, D. E. Human gut-on-a-chip inhabited by microbial flora that experiences intestinal peristalsis-like motions and flow. *Lab Chip* **12**, 2165–2174 (2012).
65. Duran-Arteaga, D., Chen, W., Rackus, D. G. & Valente, V. Selective laser etching fabrication of stacked microporous membranes for multisize particle separation in 3D microfluidics. *Sci. Rep.* **15**, 36236 (2025).
66. Choi, E. et al. Quantitatively controlled in situ formation of hydrogel membranes in microchannels for generation of stable chemical gradients. *Lab Chip* **12**, 302–308 (2012).
67. Newton, J. D. et al. Tunable in situ synthesis of ultrathin extracellular matrix-derived membranes in organ-on-a-chip devices. *Adv. Healthc. Mater.* **13**, e2401158 (2024).
68. Xue, X. et al. Generation of spatially patterned human neural tube-like structures using microfluidic gradient devices. *Nat. Protoc.* **21**, 1730–1753 (2025).
69. Xue, X. et al. A patterned human neural tube model using microfluidic gradients. *Nature* **628**, 391–399 (2024).
70. Campenot, R. B. Local control of neurite development by nerve growth factor. *Proc. Natl Acad. Sci. USA* **74**, 4516–4519 (1977).
71. Mitsuzawa, S. et al. Reduced PHOX2B stability causes axonal growth impairment in motor neurons with TARDBP mutations. *Stem Cell Rep.* **16**, 1527–1541 (2021).
72. Si, L. et al. A human-airway-on-a-chip for the rapid identification of candidate antiviral therapeutics and prophylactics. *Nat. Biomed. Eng.* **5**, 815–829 (2021).

73. Leung, C. M. et al. A guide to the organ-on-a-chip. *Nat. Rev. Methods Primers* **2**, 33 (2022).
74. Bolden, C. T. et al. Validation and characterization of a novel blood–brain barrier platform for investigating traumatic brain injury. *Sci. Rep.* **13**, 16150 (2023).
75. van Splunder, H., Villacampa, P., Martínez-Romero, A. & Graupera, M. Pericytes in the disease spotlight. *Trends Cell Biol.* **34**, 58–71 (2024).
76. Lippmann, E. S., Al-Ahmad, A., Azarin, S. M., Palecek, S. P. & Shusta, E. V. A retinoic acid-enhanced, multicellular human blood–brain barrier model derived from stem cell sources. *Sci. Rep.* **4**, 4160 (2014).
77. Zhou, X. et al. Vascular heterogeneity of tight junction Claudins guides organotropic metastasis. *Nat. Cancer* **5**, 1371–1389 (2024).
78. Barnett, S. N. et al. An organotypic atlas of human vascular cells. *Nat. Med.* **30**, 3468–3481 (2024).
79. Kim, S., Lee, H., Chung, M. & Jeon, N. L. Engineering of functional, perfusable 3D microvascular networks on a chip. *Lab Chip* **13**, 1489–1500 (2013).
80. Quintard, C. et al. A microfluidic platform integrating functional vascularized organoids-on-chip. *Nat. Commun.* **15**, 1452 (2024).
81. Liu, H. et al. A tumor-on-a-chip for in vitro study of CAR-T cell immunotherapy in solid tumors. *Nat. Biotechnol.* **44**, 959–975 (2025).
82. Menzani, B., De Gea, P., Gidrol, X. & Tubbs, E. Vascularizing organoids-on-chip for perfused and personalized models. *Lab Chip* **26**, 1798–1819 (2026).
83. Salmon, I. et al. Engineering neurovascular organoids with 3D printed microfluidic chips. *Lab Chip* **22**, 1615–1629 (2022).
84. Campisi, M. et al. Vascular STING activation facilitates NK cell anti-tumor immunity in small cell lung cancer. *Cancer Cell* **44**, 858–878 (2026).
85. Shore, A. C. Capillaroscopy and the measurement of capillary pressure. *Br. J. Clin. Pharmacol.* **50**, 501–513 (2000).
86. Skardal, A. et al. Drug compound screening in single and integrated multi-organoid body-on-a-chip systems. *Biofabrication* **12**, 025017 (2020).
87. Wang, J. et al. An eighteen-organ microphysiological system coupling a vascular network and excretion system for drug discovery. *Microsyst. Nanoeng.* **11**, 89 (2025).
88. Miller, P. G. & Shuler, M. L. Design and demonstration of a pumpless 14 compartment microphysiological system. *Biotechnol. Bioeng.* **113**, 2213–2227 (2016).
89. Esch, M. B., Ueno, H., Applegate, D. R. & Shuler, M. L. Modular, pumpless body-on-a-chip platform for the co-culture of GI tract epithelium and 3D primary liver tissue. *Lab Chip* **16**, 2719–2729 (2016).
90. Oleaga, C. et al. Multi-organ toxicity demonstration in a functional human in vitro system composed of four organs. *Sci. Rep.* **6**, 20030 (2016).
91. Boos, J. A., Misun, P. M., Michlmayr, A., Hierlemann, A. & Frey, O. Microfluidic multitissue platform for advanced embryotoxicity testing in vitro. *Adv. Sci.* **6**, 1900294 (2019).
92. Lee, H. et al. A pumpless multi-organ-on-a-chip (MOC) combined with a pharmacokinetic–pharmacodynamic (PK–PD) model. *Biotechnol. Bioeng.* **114**, 432–443 (2017).
93. LaValley, D. J., Miller, P. G. & Shuler, M. L. Pumpless, unidirectional microphysiological system for testing metabolism-dependent chemotherapeutic toxicity. *Biotechnol. Prog.* **37**, e3105 (2021).
94. Jiang, N. et al. A closed-loop modular multiorgan-on-chips platform for self-sustaining and tightly controlled oxygenation. *Proc. Natl Acad. Sci. USA* **121**, e2413684121 (2024).
95. Novak, R. et al. Robotic fluidic coupling and interrogation of multiple vascularized organ chips. *Nat. Biomed. Eng.* **4**, 407–420 (2020).
96. Yrjänäinen, A. et al. Barrier-free, open-top microfluidic chip for generating two distinct, interconnected 3D microvascular networks. *Sci. Rep.* **14**, 22916 (2024).
97. Arteel, G. E. & Naba, A. The liver matrisome—looking beyond collagens. *JHEP Rep.* **2**, 100115 (2020).
98. Bayne, E. F. et al. High-throughput extracellular matrix proteomics of human lungs enabled by photocleavable surfactant and diaPASEF. *J. Proteome Res.* **23**, 2908–2918 (2024).
99. Chaudhuri, O., Cooper-White, J., Janmey, P. A., Mooney, D. J. & Shenoy, V. B. Effects of extracellular matrix viscoelasticity on cellular behaviour. *Nature* **584**, 535–546 (2020).
100. Grindulis, K. et al. Sorption and release of small molecules in PDMS and COC for organs on chip. *Sci. Rep.* **15**, 14012 (2025).
101. Vidler, C., Crozier, K. & Collins, D. Ultra-resolution scalable microprinting. *Microsyst. Nanoeng.* **9**, 67 (2023).
102. Hsiao, K. et al. Single-digit-micrometer-resolution continuous liquid interface production. *Sci. Adv.* **8**, eabq2846 (2022).
103. Lipkowitz, G. et al. Injection continuous liquid interface production of 3D objects. *Sci. Adv.* **8**, eabq3917 (2022).
104. Cook, S. R., Ball, A. G., Mohammad, A. & Pompano, R. R. A 3D-printed multi-compartment organ-on-chip platform with a tubing-free pump models communication with the lymph node. *Lab Chip* **25**, 155–174 (2025).
105. Lohasz, C., Rousset, N., Renggli, K., Hierlemann, A. & Frey, O. Scalable microfluidic platform for flexible configuration of and experiments with microtissue multiorgan models. *SLAS Technol.* **24**, 79–95 (2019).
106. Jian, T. H. Z. et al. Physiological perfusion of human vasculature reveals a YAP/TAZ-Apelin switch linking intraluminal flow to endothelial state transitions and vessel remodeling. Preprint at *bioRxiv* https://doi.org/10.64898/2026.03.21.713033 (2026).
107. Maschmeyer, I. et al. A four-organ-chip for interconnected long-term co-culture of human intestine, liver, skin and kidney equivalents. *Lab Chip* **15**, 2688–2699 (2015).
108. Floryan, M. et al. Long-term physiological flow rescues regressed microvascular networks and increases their longevity. *npj Biol. Phys. Mech.* **2**, 24 (2025).
109. DeMeo, B. et al. Active learning framework leveraging transcriptomics identifies modulators of disease phenotypes. *Science* **390**, eadi8577 (2025).
110. Li, Y. et al. SOAR elucidates biological insights and empowers drug discovery through spatial transcriptomics. *Sci. Adv.* **11**, eadt7450 (2025).
111. Reinecke, M. et al. Chemical proteomics reveals the target landscape of 1,000 kinase inhibitors. *Nat. Chem. Biol.* **20**, 577–585 (2024).
112. Xu, T., Zhao, H., Wang, M., Chow, A. & Fang, M. Metabolomics and in silico docking-directed discovery of small-molecule enzyme targets. *Anal. Chem.* **93**, 3072–3081 (2021).
113. Dekkers, J. F. et al. High-resolution 3D imaging of fixed and cleared organoids. *Nat. Protoc.* **14**, 1756–1771 (2019).
114. Beghin, A. et al. Automated high-speed 3D imaging of organoid cultures with multi-scale phenotypic quantification. *Nat. Methods* **19**, 881–892 (2022).
115. Yasuhiko, O., Takeuchi, K., Yamada, H. & Ueda, Y. Multiple-scattering suppressive refractive index tomography for the label-free quantitative assessment of multicellular spheroids. *Biomed. Opt. Express* **13**, 962–979 (2022).
116. Kim, G. et al. Holotomography. *Nat. Rev. Methods Primers* **4**, 51 (2024).
117. Park, J. et al. Clinical translation of photoacoustic imaging. *Nat. Rev. Bioeng.* **3**, 193–212 (2025).
118. Huang, K. et al. High-speed photoacoustic and ultrasonic computed tomography of the breast tumor for early diagnosis with enhanced accuracy. *Sci. Adv.* **11**, eadz2046 (2025).

119. Suzuki, Y. et al. Photoacoustic lymphangiography exhibits advantages over near-infrared fluorescence lymphangiography as a diagnostic tool in patients with lymphedema. *J. Vasc. Surg. Venous Lymphat. Disord.* **10**, 454–462 (2022).
120. Huynh, N. T. et al. A fast all-optical 3D photoacoustic scanner for clinical vascular imaging. *Nat. Biomed. Eng.* **9**, 638–655 (2025).
121. Barulin, A. et al. Axially multifocal metalens for 3D volumetric photoacoustic imaging of neuromelanin in live brain organoid. *Sci. Adv.* **11**, eadr0654 (2025).
122. Scholler, J. et al. Dynamic full-field optical coherence tomography: 3D live-imaging of retinal organoids. *Light Sci. Appl.* **9**, 140 (2020).
123. Pike, C. M. et al. High-throughput assay for predicting diarrhea risk using a 2D human intestinal stem cell-derived model. *Toxicol. In Vitro* **106**, 106040 (2025).
124. Venz, A., Duckert, B., Lagae, L., Takalloo, S. E. & Braeken, D. Impedance mapping with high-density microelectrode array chips reveals dynamic heterogeneity of in vitro epithelial barriers. *Sci. Rep.* **15**, 1592 (2025).
125. Lefebvre, C. et al. Integration of microfluidic devices with microelectrode arrays to functionally assay amyloid-β-induced synaptotoxicity. *ACS Biomater. Sci. Eng.* **10**, 1856–1868 (2024).
126. Varma, S. & Voldman, J. A cell-based sensor of fluid shear stress for microfluidics. *Lab Chip* **15**, 1563–1573 (2015).
127. Mark, C. et al. Collective forces of tumor spheroids in three-dimensional biopolymer networks. *eLife* **9**, e51912 (2020).
128. Kanade, P. P. et al. MEA-integrated cantilever platform for comparison of real-time change in electrophysiology and contractility of cardiomyocytes to drugs. *Biosens. Bioelectron.* **216**, 114675 (2022).
129. Bliley, J. M. et al. Dynamic loading of human engineered heart tissue enhances contractile function and drives a desmosome-linked disease phenotype. *Sci. Transl. Med.* **13**, eabd1817 (2021).
130. Sala, L. et al. MUSCLEMOTION: a versatile open software tool to quantify cardiomyocyte and cardiac muscle contraction in vitro and in vivo. *Circ. Res.* **122**, e5–e16 (2018).
131. Ansaryan, S. et al. High-throughput spatiotemporal monitoring of single-cell secretions via plasmonic microwell arrays. *Nat. Biomed. Eng.* **7**, 943–958 (2023).
132. Ansaryan, S. et al. Spatiotemporal interrogation of single spheroids using multiplexed nanoplasmonic-fluorescence imaging. *Small Methods* **9**, 2500106 (2025).
133. Liu, Y.-C. et al. Nanoplasmonic single-tumoroid microarray for real-time secretion analysis. *Adv. Sci.* **11**, 2401539 (2024).
134. Rantataro, S., Parkkinen, I., Airavaara, M. & Laurila, T. Real-time selective detection of dopamine and serotonin at nanomolar concentration from complex in vitro systems. *Biosens. Bioelectron.* **241**, 115579 (2023).
135. Johansson, P. K., Liu, Y., Klett, K. C., Heilshorn, S. C. & Enejder, A. Polarized distribution of lipid droplets with long acyl chains and unsaturation are hallmarks of human intestinal enteroid differentiation. *Anal. Chem.* **97**, 27076–27090 (2025).
136. Liu, Y. et al. Engineered hydrogels for organoid models of human nonalcoholic fatty liver disease. *Adv. Sci.* **12**, e17332 (2025).
137. Pope, I. et al. Identifying subpopulations in multicellular systems by quantitative chemical imaging using label-free hyperspectral CARS microscopy. *Analyst* **146**, 2277–2291 (2021).
138. Tan, S. et al. Development of an AI model for DILI-level prediction using liver organoid brightfield images. *Commun. Biol.* **8**, 886 (2025).
139. Kok, R. N. U., Spoelstra, W. K., Betjes, M. A., van Zon, J. S. & Tans, S. J. Label-free cell imaging and tracking in 3D organoids. *Cell Rep. Phys. Sci.* **6**, 102522 (2025).
140. Liu, H. et al. A large model-derived algorithm for complex organoids with internal morphogenesis and digital marker derivation. *Anal. Chem.* **96**, 19258–19266 (2024).
141. Yang, X. et al. A live-cell image-based machine learning strategy for reducing variability in PSC differentiation systems. *Cell Discov.* **9**, 53 (2023).
142. Asano, T. et al. A deep learning approach to predict differentiation outcomes in hypothalamic-pituitary organoids. *Commun. Biol.* **7**, 1468 (2024).

Acknowledgements

The authors acknowledge support from the Kleberg Foundation Medical Research Grant Program and the Gootter-Jensen Foundation. Because of space constraints, the authors apologize for not including all relevant citations.

Author contributions

J.L. and J.C.W. conceptualized the manuscript and wrote the first draft. S.M.G., J.T.C. and S.C.H. edited the subsequent drafts.

Funding

This work was supported by the National Institutes of Health (grant numbers U01 AI195484, U01 AI183953, UG3 TR005845, UG3 AG097135 and UM1 TR006031 to J.C.W.; R61 CA278450 and R01 MH137333 to S.C.H.) and the National Science Foundation (grant number DMR 2427971 to S.C.H.).

Competing interests

J.C.W. is a co-founder and scientific advisory board member of Greenstone Biosciences. The remaining authors declare no competing interests.

Additional information

Correspondence and requests for materials should be addressed to Joseph C. Wu.

Peer review information *Nature Biomedical Engineering* thanks Olujimi Ajijola and the other, anonymous, reviewer(s) for their contribution to the peer review of this work.

Reprints and permissions information is available at www.nature.com/reprints.

Publisher's note Springer Nature remains neutral with regard to jurisdictional claims in published maps and institutional affiliations.

Springer Nature or its licensor (e.g. a society or other partner) holds exclusive rights to this article under a publishing agreement with the author(s) or other rightsholder(s); author self-archiving of the accepted manuscript version of this article is solely governed by the terms of such publishing agreement and applicable law.

© Springer Nature Limited 2026